On the nitrogen-induced lattice expansion of a non-stainless austenitic steel, Invar 36®, under triode plasma nitriding

Tao, Xiao; Matthews, Allan; Leyland, Adrian

DOI:
10.1007/s11661-019-05526-0

Document Version
Peer reviewed version

Citation for published version (Harvard):
Tao, X, Matthews, A & Leyland, A 2020, 'On the nitrogen-induced lattice expansion of a non-stainless austenitic steel, Invar 36®, under triode plasma nitriding', *Metallurgical and Materials Transactions A*, vol. 51, no. 1, pp. 436-447. https://doi.org/10.1007/s11661-019-05526-0

On the nitrogen-induced lattice expansion of a non-stainless austenitic steel, Invar 36®, under Triode Plasma Nitriding

Authors:

Xiao Tao[a,c], Allan Matthews[b], Adrian Leyland[a]

[a] Department of Materials Science and Engineering, The University of Sheffield, Sheffield, S1 3JD, UK

[b] School of Materials, The University of Manchester, Manchester, M13 9PL, UK

[c] School of Metallurgy and Materials, University of Birmingham, Birmingham B15 2TT, UK

Xiao Tao, email: x.tao@bham.ac.uk

Allan Matthews, email: allan.matthews@manchester.ac.uk

Adrian Leyland, email: a.leyland@sheffield.ac.uk

*Corresponding author: Dr. Adrian Leyland

Email: a.leyland@sheffield.ac.uk

Telephone: +44 (0) 114 222 5486

Fax: +44 (0) 114 222 5943

Full postal address: Department of Materials Science and Engineering, Sir Robert Hadfield Building, Mappin Street, Sheffield, S1 3JD, United Kingdom

Abstract

Chromium, as a strong nitride forming element, is widely regarded to be an 'essential' ingredient for the formation of a nitrogen-expanded lattice in thermochemical nitrogen diffusion treatments of austenitic (stainless) steels. In this paper, a proprietary 'chrome-free' austenitic iron-nickel alloy, Invar® 36 (Fe-36Ni, in wt.%), is characterised after Triode-Plasma Nitriding (TPN) treatments at 400-450°C and compared to a 'stainless' austenitic counterpart RA 330® (Fe-19Cr-35Ni, in wt.%) treated under equivalent nitriding conditions. Cr does indeed appear to play a pivotal role in colossal nitrogen supersaturation (and hence, anisotropic lattice expansion and superior surface hardening) of austenitic steel under low-temperature ($\leq$ 450°C) nitrogen diffusion. Nevertheless, this work reveals that nitrogen-induced lattice expansion occurs below the nitride-containing surface layer in Invar 36 alloy after TPN treatment, implying that Cr is not a necessity for the nitrogen-interstitial induced lattice expansion phenomenon to occur, also suggesting another type of γ_N.

Keywords: austenitic steel; expanded austenite; plasma nitriding

1 Introduction

After early scientific studies published by Bell et al. [1] and Ichii et al. [2] in the 1980s, low temperature plasma diffusion treatments have been widely investigated as a potential solution to the poor tribological performance of Austenitic Stainless Steels (ASSs) [3-7]. Nitrogen-expanded austenite [3] (γ_N; also called "S-phase" [2]) can be synthesized on ASSs (such as AISI 304, 310 and 316 type alloys, based mainly on the Fe-Cr-Ni ternary alloy system) under low temperature ($\leq 450°C$) nitriding without the formation of chromium nitride, where the original face-centred cubic (FCC) structure is expanded anisotropically under extremely high interstitial nitrogen uptake [8-10]. Recent studies of expanded austenite (γ_N) have focused on the crystallographic structure of N-supersaturated ASS surfaces [11-18]; however, there are still uncertainties about the roles of the primary substitutional alloying elements (e.g. Cr, Ni and/or Mn) in the formation of γ_N during low temperature thermochemical diffusion treatment. This topic can be traced back to the 1990s, when authors such as Menthe et al. [19] and Yasumaru [20] reported that γ_N does not form in steels containing either Cr or Ni/Mn alone (i.e. Fe-13Cr-0.2C, Fe-17Cr-0.1C, Fe-30Ni, Fe-32Ni, Fe-42Ni and Fe-26Mn-0.2C, in wt.%) under low-temperature nitriding. It was argued that both Cr and Ni/Mn are necessary for the formation of γ_N on austenitic steels. More recently, however, Buhagiar et al. [13] and Tao et al. [18] reported the formation of γ_N on Ni-free high-Mn ASSs, proving unequivocally that neither Ni nor Mn are in themselves crucial for the formation of γ_N (although each may affect differently the nitrogen supersaturation levels obtained, the lattice plasticity mechanisms and the γ_N lattice (in)stability observed with increasing treatment temperature/time [18]).

On the other hand, Cr − as a strong nitride forming element − is widely believed to be an 'essential' component of the substrate alloy composition for γ_N formation (with appropriate

mechanical/tribological/corrosion resistant properties) [21, 22]. Expanded austenite has been synthesized using various low-temperature nitrogen surface modification techniques on Fe/Ni/Co-based alloys with substrate Cr content ranging from ~13 at.% (for proprietary precipitation hardening stainless steels, such as Nanoflex® and Corrax® [23]) to ~31 at.% (for a special Co-Cr alloy [24]). A significant amount of Cr (as a 'nitrogen trapper') in the substrate (i.e. ≥ 12 at.%, also typical for stainless steels to promote the stable surface chromium oxide layer formation) appears to be important in the formation of 'useful' γ_N under low-temperature nitrogen surface modification. The role of Cr has been investigated and discussed in several studies of γ_N-304 and/or γ_N-316, which have pointed to 'trapping and detrapping' diffusion of N [25, 26] and to the bonding (and short-range ordering) of N to Cr [19, 27, 28]. It was postulated that Cr could provide trap sites for N, contributing to the extremely high interstitial absorption and anomalous (anisotropic) lattice expansion of ASSs, seen under low-temperature nitriding [10, 22, 28]. Additionally, pure γ-Ni clearly shows no lattice expansion under nitrogen ion implantation [29, 30], but γ_N was reported (with evident XRD peak shifts to lower 2θ angles) after nitrogen surface modification treatments on Ni-alloys that contain strong-nitride formers, such as Ni-Cr binary alloys (containing ~20 at.% Cr [29, 30] and ~26 at.% Cr [31]), Ni-Ti binary alloys (containing ~1.6 at.% Ti [32], ~3.3 at.% Ti [32] and ~5.8 at.% Ti [31]), and a range of commercial Cr-containing Ni-superalloys [29]. While a (meta)stable austenitic substrate microstructure alone appears an insufficient requirement, strong-nitride-formers appear to be a necessity for the formation of γ_N on Fe/Ni/Co-based substrates.

Nevertheless, Williamson et al. [29] reported 'highly-expanded' and 'less-expanded' FCC phases (designated as γ_{N1} and γ_{N2}, respectively, in their paper) on a Cr-free high-Ni Invar alloy (Fe-35Ni, in wt.%) after N-implantation at 400°C, which appears to be contradictory

(and hence intriguing) to the widely-reported 'essential' role played by Cr in austenite lattice expansion under low-temperature nitrogen diffusion treatment. However, apart from surface XRD profiles, no further details were given in [29] on the structure of expanded austenitic phases synthesized on Fe-35Ni. Alloy RA 330® (Fe-19Cr-35Ni, in wt.%), as a high-Ni stainless counterpart of Fe-35Ni, was previously characterised by the authors of the present work after triode-plasma nitriding (TPN) [18]. To investigate the γ_{N1} and γ_{N2} phases reported in [29] and to elucidate the role of Cr, a TPN-treated non-stainless high-Ni austenitic steel, Invar 36® (Fe-36Ni, in wt.%), is investigated in this study and compared (under equivalent treatment conditions) to the TPN-treated alloy RA 330.

2 Experimental

Table I. Material composition, in wt.%

Material	Specification	Fe	Cr	Ni	Mn	C	Others
Invar 36®[a]	ASTM F1686-06, UNS K93603	Bal.	0.07	36.08	0.4	0.04	0.14 Si, 0.04 Co
RA 330®[b]	ASTM B536-07 UNS N08330	Bal.	18.5	34.9	1.4	0.05	0.16 Al, 0.14 Ti, 0.11 Cu, 1.2 Si, 0.01N

[a]Composition of Invar 36® is presented according to the original material supplier Deutsche Nickel Gmbh and it also contains 0.032 wt.% (in total) of minor alloying additions of Al, Mg, Ti and Zr; The Ni content was confirmed using SEM-EDX.

[b]Composition of RA 330® is presented according to the original material supplier ATI Allegheny Ludlum Corporation; the contents of major alloying elements (i.e. Cr, Ni, Mn and Si) were confirmed using SEM-EDX.

The chemical compositions of Invar 36® (City Special Metals Ltd. Sheffield, UK) and RA 330® (Neonickel Ltd. Blackburn, UK) are presented in **Table I**. Disks of 20 mm diameter (and 3 mm thick) were sliced from a solution-annealed bar of alloy Invar 36 using an

abrasive cutting wheel (Struers Secotom-50). Rectangular RA 330 alloy coupons of dimensions ~25×25×4 mm were cut from 4 mm thick solution-annealed plates. Invar 36 samples were plasma nitrided in a modified commercial PVD coating unit, Tecvac IP70L, using a triode-plasma nitriding (TPN) configuration [3, 33, 34] under a treatment pressure of 0.4 Pa (with N_2:Ar gas volume ratio of 7:3) and substrate bias of -200 V, at 400°C, 425°C and 450°C for 4hrs and 20hrs, respectively. The precise sample preparation and nitriding treatment procedures are described in detail in Ref. [18].

A Nikon Eclipse LV150 optical microscope (OM) was used for optical imaging and a Philips XL30S FEG electron microscope (with Oxford Instruments INCA EDX system) for Energy Dispersive X-ray (EDX) spectroscopy. Beam acceleration voltage and spot size were 15kV and 5, respectively. Beam intensity was calibrated with a cobalt standard before each measurement. The mean surface compositions were evaluated from 10 random measurements over the material surface, where each measurement location covered an area of 65×45 μm^2. Back-Scattered Electron (BSE) images were taken from polished sample cross-sections using an FEI Nova NanoSEM 450 instrument at a beam acceleration voltage of 20 kV and spot size of 5.5. Vickers indentation hardness was evaluated using a Struers Durascan® 70 hardness tester. The indentation load and dwell time were 0.025 kg and 15 s, respectively. The mean material surface hardness, $HV_{0.025}$, was averaged from 12 randomly-distributed indents. Nanoindentation hardness measurements were performed on polished sample cross-sections using a Hysitron TriboScope® Nanoindentor (≤5 mN load, Berkovich diamond indenter). The displacements of indentations from the sample surface were measured in-situ using an atomic force microscope attached to the nanoindentor. The mean hardness value at each depth level was averaged from 5 indentations.

X-ray diffraction analysis was performed at two-theta angles from 30° to 80° in Bragg-Brentano geometry using a Bruker D2 PHASER (30 kV, 10 mA, Cu-$K\alpha_{ave}$ 0.1542 nm) and in Seeman-Bohlin geometry at 2° Glancing Angle (GAXRD) using a PANalytical X'pert^3 instrument (45 kV, 40 mA; monochromated Cu$K\alpha_1$ 0.1541 nm). The 400°C 20hrs nitrided and 450°C 20hrs nitrided Invar samples were also ground using P1200 SiC paper to successively remove ~3/5/10/20/30 μm of treatment layer (measured using a micrometer) and were examined respectively under GAXRD to determine the evolution of phase structure with treatment depth. Cross-sectional thin foils for Transmission Electron Microscopy (TEM) were prepared via Focused Ion Beam (FIB) milling using an FEI Quanta 200 3D electron microscope with 30kV gallium ion beam attachment, as described previously [18]. The thinned areas were examined under a Philips EM420 transmission electron microscope at a beam acceleration voltage of 120 kV. Scanning TEM (STEM) analysis was carried out using a FEI Philips Tecnai F20 electron microscope. STEM-EDX analysis was performed at 200 kV and a spot size of 6 (with Oxford Instruments AZtec EDX software).

3 Results

3.1 Cross-sectional backscattered electron images and hardness-depth profiles

All nitrided Invar 36 surfaces show a discontinuous, feature-containing surface layer in **Fig. 1** (see **Figure A1** in **Appendix** for BSE images of lower magnification). Neither the penetration depths nor the distributions of these features on nitrided Invar are homogenous. At a treatment temperature of 400°C, the dark features start forming from the very surface of material (**Fig. 1a**) and then grow and coalesce with treatment time (**Fig. 1d**). 'Cellular' regions are observed in Invar 36 TPN-treated at 425°C and 450°C. These cellular regions are composed of laminates of two different phases, with an interlamellar spacing of several tens of nanometers. Owing to the large discrepancy in atomic mass between interstitial nitrogen

atoms and substitutional metal atoms (i.e. 14 for N, 55.8 for Fe and 58.7 for Ni), the features observed on sample cross-sections of Invar 36 under backscattered electron (BSE) imaging (**Fig. 1**) mainly originate from the inhomogeneous distribution of nitrogen following TPN treatment. Under BSE imaging in **Fig. 1**, lower mean atomic weight yields less electron scattering, so the N-rich phase appears dark (and will be identified in the following **Section 3.3**). It should also be mentioned that the black wavy features (in **Fig. 1f**) are cracks and this feature is clearly shown in the FIB-TEM sample in **Section 3.2**.

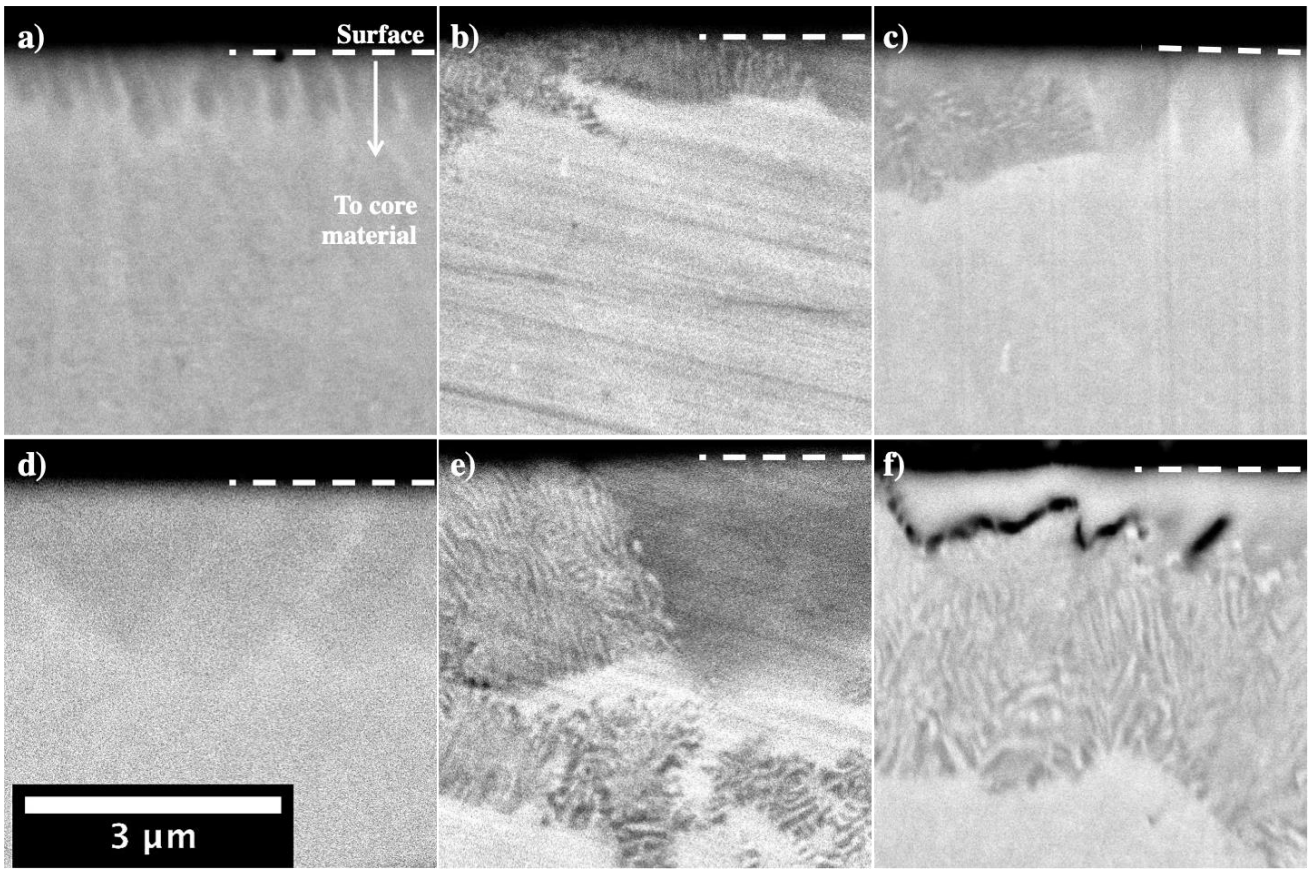

Fig. 1 Cross-sectional BSE images of Invar 36® after plasma nitriding at a) 400°C 4hrs, b) 425°C 4hrs, c) 450°C 4hrs, d) 400°C 20hrs, e) 425°C 20hrs, f) 450°C 20hrs

The hardness-depth profiles of nitrided Invar (**Fig. 2a**) indicate total case depths of ~11 µm and ~24 µm after treatments at 400°C and 450°C, respectively. Hardness profiles of nitrided Invar first drop steeply after leaving the nitride-containing surface layer and then gradually

reduce as approaching towards core. The hardened layers on nitrided Invar are clearly thicker than the feature-containing layers (observed in BSE images, **Fig. 1d, f**) would suggest and correspond to deep nitrogen diffusion zones (see **Section 3.3**).

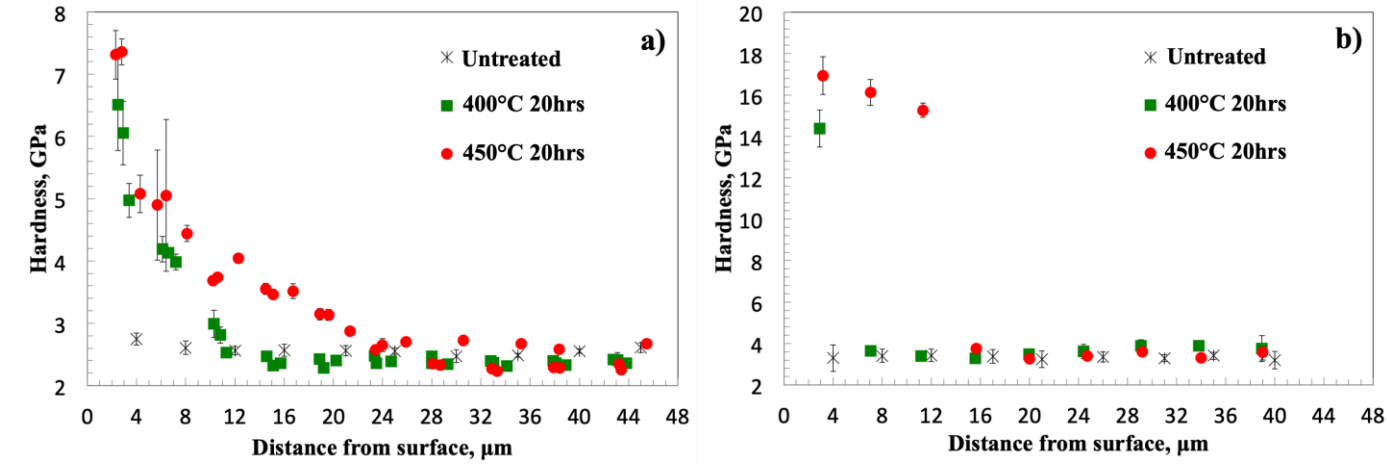

Fig. 2 Cross-sectional nanoindentation hardness-depth profiles of a) Invar 36® and b) RA 330® before and after TPN at 400°C and 450°C for 20hrs (error bars − ± 95% confidence interval at each depth level)

In contrast, homogenous γ_N-330 layers were observed on alloy RA 330 after equivalent nitriding treatments [18]. The hardened case depths on TPN-treated RA 330 in **Fig. 2b** are consistent with the observed layer depths, i.e. ~4 µm at 400°C and ~14 µm at 450°C [18]. Compared to the hardness-depth profile of nitrided Invar (**Fig. 2a**), γ_N-330 layers (synthesized under equivalent treatment conditions) are much harder (but significantly thinner) and present an abrupt drop in hardness at the layer/core interface (a characteristic feature of N-supersaturated austenite layers on stainless steel surfaces [22, 35]).

3.2 Phase identification

XRD and GAXRD

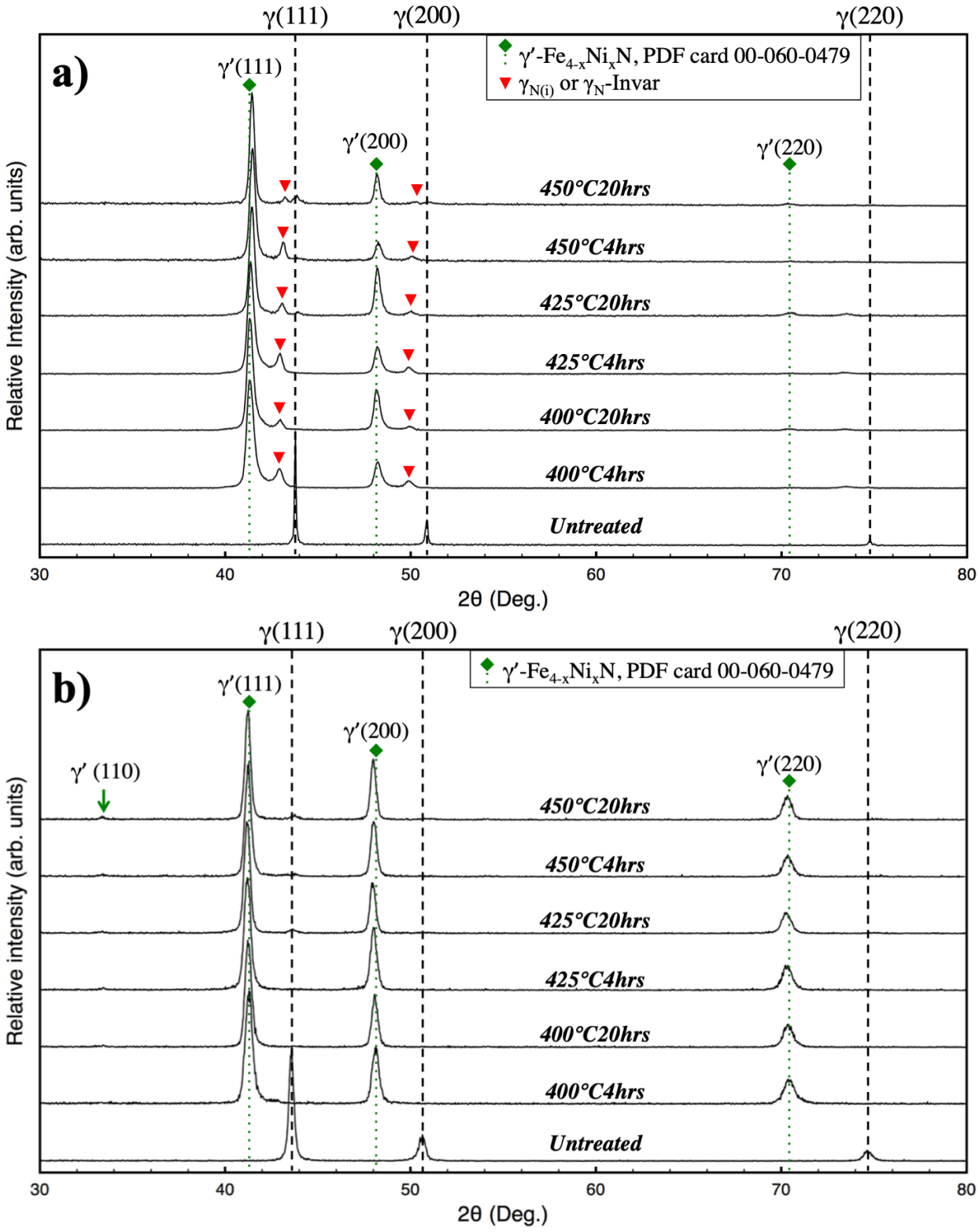

Fig. 3 a) Theta-2theta XRD and b) GAXRD profiles of TPN-treated Invar 36®

The XRD profiles of nitrided Invar 36 in **Fig. 3a** appear analogous to that reported for Invar 36 under nitrogen ion beam processing by Williamson et al. [29], showing "highly-expanded and less-expanded FCC structures" after treatment − where both expanded structures have almost ideal FCC structure (as determined from the 111 and 220 peak positions). Firstly, under both θ-2θ XRD (**Fig. 3a**) and GAXRD (**Fig. 3b**), the peak positions of the 'highly-expanded' FCC structure match with the $Fe_{4-x}Ni_xN$, PDF card 00-060-0479, stable for $0 < x < 3.3$ under experimental conditions [36]). This highly-expanded FCC structure (in **Fig. 3**) could be identified as Fe_4N-type γ′-nitride. Different to the θ-2θ XRD profiles of TPN-treated Invar (**Fig. 3a**), the GAXRD profiles of the same materials (**Fig. 3b**) reveal only the 'highly-expanded FCC' phase (i.e. γ′-nitride) without the 'less-expanded' FCC phase. Considering the shallow X-ray attenuation depth under GAXRD, γ′-nitride should correspond to a phase located close to surface, with the 'less-expanded' phase formed deeper in the diffusion zone. Then, the features observed in the near surface of nitrided Invar in **Fig. 1** can be attributed to the formation of γ′-nitride. Additionally, an unexpanded γ(111) peak (near 43.5°) is also seen on Invar after 20hrs treatment at 425°C and 450°C (**Fig. 3**), which could be correlates well the (bright) N-depleted lamellae in 'cellular' region.

To reveal the surface phases on nitrided Invar (typically, the 'less-expanded FCC structure') that contribute to deep hardened zones in **Fig. 2a**, the 400°C 20hrs and 450°C 20hrs nitrided Invar samples were further investigated under GAXRD before and after successive layer removal, as shown in **Fig. 4**. The γ′ peaks were observed on both samples to a depth of ~3 μm. At a depth of ~3 μm, unexpanded γ peaks are evident on Invar after TPN for 20hrs at 450°C, but are not observed after 20hrs treatment at 400°C. These unexpanded γ peaks at ~3 μm depth on the 450°C and 20hrs treated Invar alloy appear to correspond to the bright N-depleted lamellar phase in the 'cellular' region in **Fig. 1f**.

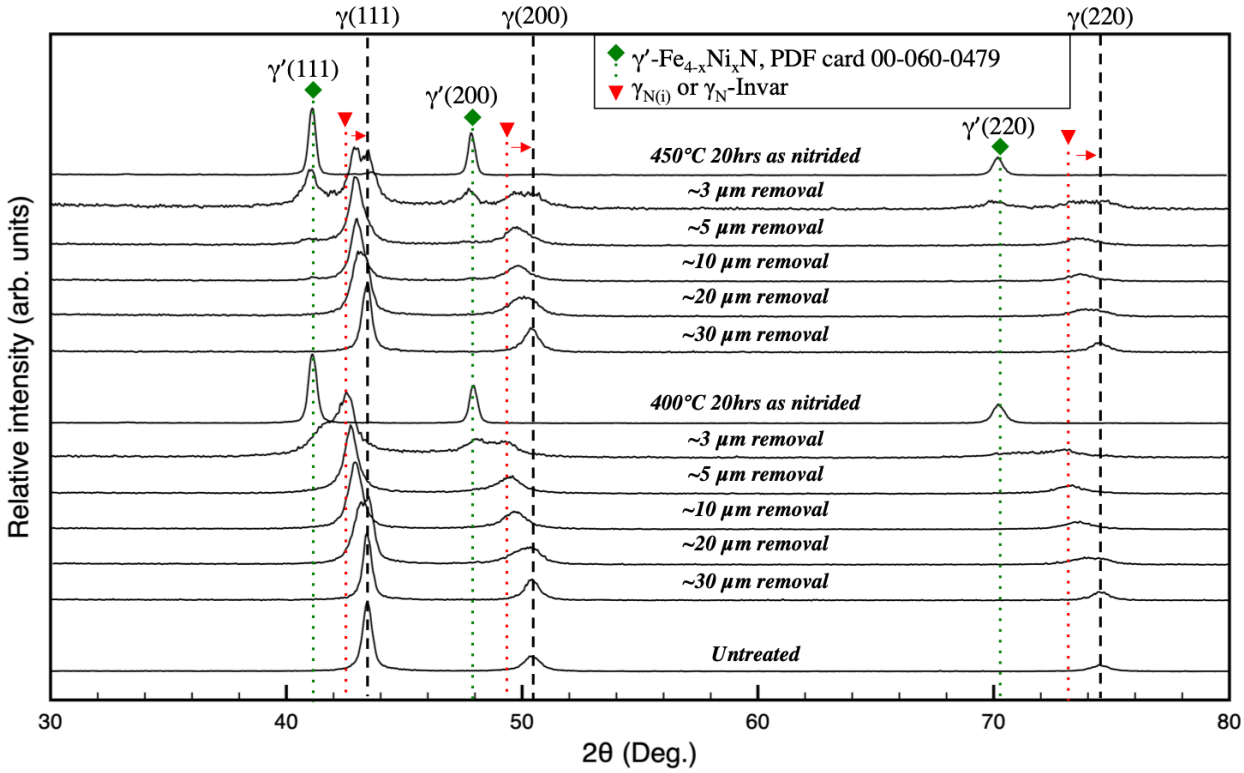

Fig. 4 GAXRD profiles of the 400°C 20hrs and the 450°C 20hrs nitrided Invar 36® before and after successive layer removal, as compared to the untreated sample

More importantly, below the γ′-containing surface zones, the 'less-expanded FCC structure' is clearly revealed at depths from ~3 to 20 μm with continuous XRD peak shifts to higher 2θ angles from surface to core (towards the peak positions of substrate austenite, as indicated by red arrows in **Fig. 4**), until the unmodified core is reached at a depth of ~30 μm. The 'less-expanded FCC structure', γ_N-Invar, appears to be continuously expanded from the parent austenite under the insertion of interstitial nitrogen. The gradual shift of γ_N-Invar peaks to higher 2θ angles with increasing depth could be attributed to the commensurate reduction of nitrogen in solid solution from surface to core, which also leads to a gradually reducing hardness with depth in the γ_N-Invar regions (**Fig. 2a**).

FIB-TEM

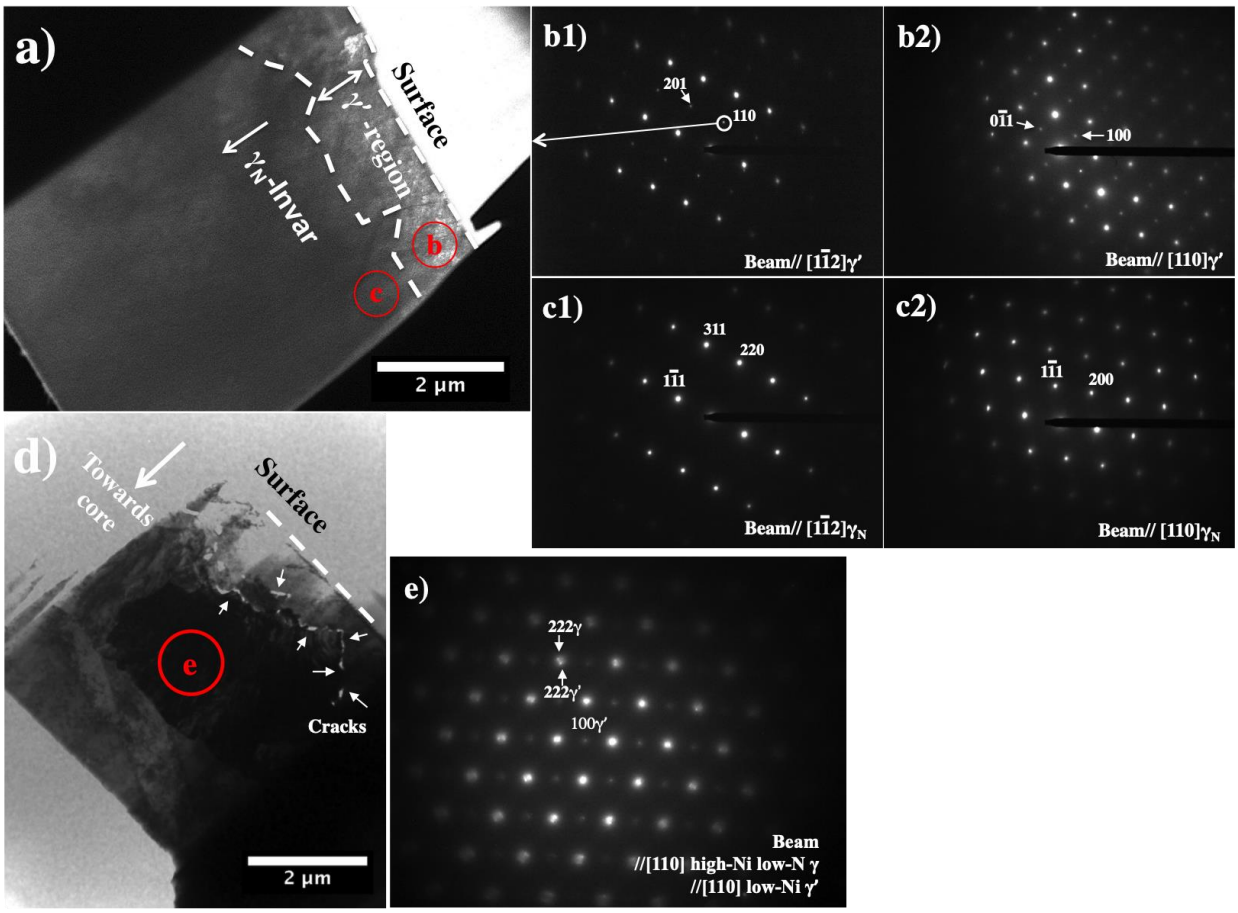

Fig. 5 a) DF-TEM image of 400°C 20hrs nitrided Invar, constructed with 110 γ′ diffraction electrons as indicated in Fig. 5b1; b1,2) SAEDs of region b; c1,2) SAEDs of region c; d) BF-TEM image of 450°C 20hrs nitrided Invar; e) SAED of region e

Cross-sectional TEM samples of 400°C and 450°C 20hrs nitrided Invar surfaces were also prepared and investigated. Extra 'forbidden' FCC spots are revealed for γ′ (**Fig 5b1, 2** and **Fig. 5e**), but not for γ_N-Invar (**Fig 5c1, 2**), in good agreement with the weak γ′(110) GAXRD peaks observed in **Fig. 3b**. At a treatment temperature of 400°C, topmost γ′ is revealed under DF-TEM imaging using γ′(110) diffraction electrons that γ′ appears slightly brighter than the underlying γ_N-Invar **(Fig 5a)**. This topmost γ′-nitride shares the same crystal orientation as the underlying γ_N-Invar, with a cubic-to-cubic structure-orientation relationship, in which case γ′ appears to be transformed from γ_N-Invar via interstitial-nitrogen ordering (into an Fe_4N-type structure) during TPN.

There are different colonies of phase mixtures in the intermediate cellular regions on 450°C and 20hrs TPN-treated Invar. The selected area EDP of a colony (i.e. the dark region in the middle of **Fig. 5d**) presents two sets of FCC diffraction spots (**Fig. 5e**), suggesting a cubic-to-cubic orientation relationship and a lattice parameter ratio of ~1.05 (as determined from electron diffraction distances) between two phases. Taking one of the phases in the phase mixture as being γ′-nitride (lattice parameter of 0.3789 nm, PDF card 00-060-0479), the lattice parameter of the other FCC phase can be estimated as ~0.3609 nm, which is very close to the lattice parameter of ~0.3606 nm measured for untreated austenite, as determined from the 111 peak positions from GAXRD profiles in **Fig. 4**. Together with the γ′ and unexpanded XRD peaks observed for the 450°C TPN-treated Invar at ~3 μm depth in **Fig. 4**, the phase mixture appears to be γ′ and unexpanded γ. These colonies of phase mixtures do not share the same crystal orientation to each other. No consistent crystallographic relation was observed between the colony of phase mixture in **Fig. 5d** and the underlying (and probably the parent) γ_N-Invar. The formation of these phase mixtures is likely to occur via nucleation and growth of γ′. Additionally, cracks are observed and indicated with white arrows in **Fig. 5d**. These micro-cracking are believed associated with the formation of γ′.

Furthermore, the lamellar phase mixture on Invar nitride at 450°C and 20hrs can clearly be seen in HAADF imaging (**Fig. 6a**). STEM-EDX analysis of the phase mixture (**Fig. 6**) indicates redistribution of both interstitial nitrogen and substitutional metallic elements (e.g. Fe with Ni). Compared to the adjacent N-depleted regions, the N-rich regions exhibit higher Fe content (**Fig. 6b**) but lower Ni content (**Fig. 6c**). Given that γ′-$Fe_{4-x}Ni_xN$ is stable for $0 < x < 3.3$ [36], the γ′ formed in cellular regions have different composition (i.e. much lower Ni content) to those uniform γ′ phases that formed via interstitial ordering (probably γ′-

$Fe_{2.6}Ni_{1.4}N$, at x ≈ 1.4 considering 35 at.% Ni). The high-Ni γ phase (adjacent to low-Ni γ′) could still contain a very small amount of residual nitrogen, such that the γ phase in the cellular region has a different composition to γ-Invar – and could therefore possess a different lattice parameter. Thus, the phase mixture in cellular regions could be attributed to local eutectoid decomposition of γ_N-Invar to an intimate mixture of lamellar low-Ni γ′ and high-Ni, low-nitrogen γ. Additionally, minor alloying elements (such as Cr, Mn, Si, Co and C, see **Table I.**) could also re-distribute between the two phases in this cellular region; however, probably owing to their low concentrations, such re-distribution was not clearly visible in the EDX analysis (see for example Cr in **Fig. 6e**).

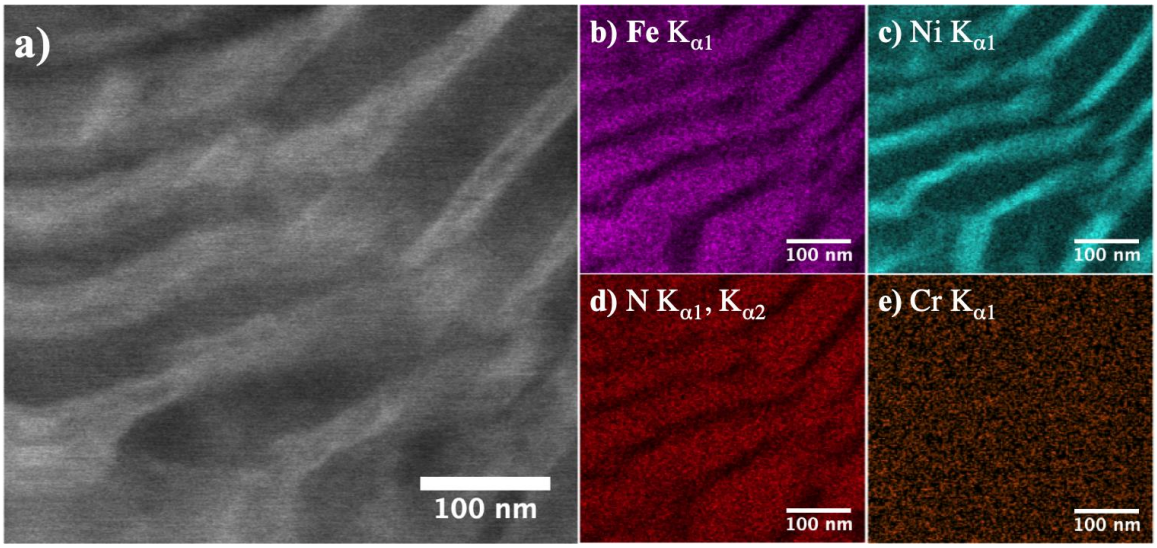

Fig. 6 a) HAADF image showing the lamellar phase mixture, STEM-EDX maps of the region for b) Fe (Kα1), c) Ni (Kα1), d) N (Kα1 and Kα2) and e) Cr (Kα1)

3.3 Surface nitrogen content and hardness

Surface nitrogen contents of nitrided Invar samples (**Table II.**) ranged from ~18 to ~20 at.%, which is significantly higher than the maximum equilibrium N-solubility limit in γ-Fe (i.e. ~10.3 at.% at ~650°C [37]), but lower than the surface nitrogen content of the nitrided alloy

RA 330 (ranging from ~23 to 26 at.%) [18]. The presence of Cr in the austenitic lattice of alloy RA 330 does appear to be beneficial in obtaining a higher surface nitrogen uptake. Surface N content of Invar samples does not vary significantly with treatment temperature and time, which could be attributed to the formation of γ′ nitride at the substrate surface.

Table II. Surface nitrogen content and hardness

	Surface at.% Nitrogen	**Surface hardness, $HV_{0.025}$**	
	Invar 36®	*Invar 36®*	*RA 330®*
Untreated	/	200 ± 3	210 ± 4
400°C 4hrs	18.3 ± 0.4	390 ± 5	520 ± 10
400°C 20hrs	19.8 ± 0.3	498 ± 8	1048 ± 62
425°C4hrs	18.9 ± 0.3	531 ± 8	515 ± 17
425°C 20hrs	20.6 ± 0.3	705 ± 25	1494 ± 21
450°C 4hrs	18.8 ± 0.6	638 ± 8	786 ± 26
450°C 20hrs	19.6 ± 0.6	734 ± 12	1573 ± 18

*Values of surface nitrogen content and layer depths are shown as mean ± 95% confidence interval; Surface nitrogen contents of nitrided RA 330® were shown in Ref. **18**

Both alloys exhibit significant hardening after TPN treatment (**Table II.**) and the hardening effect increases with treatment temperature and/or time. Maximum Vickers surface hardness was achieved at the upper treatment condition (of 450°C for 20hrs) for both alloys. The hardness values obtained are influenced by different factors, such as nitrogen composition-depth profile, phase distribution, indent penetration depth and nitride layer depth. The increase in surface hardness for TPN-treated Invar with treatment temperature and time could be attributed to: i) the growth of a diffusion zone, ii) the development of uniform γ′-$Fe_{2.6}Ni_{1.4}N$ phase at material surface, and iii) the lamellar phase mixtures that contain fine lamella of low-Ni γ′ and high-Ni (low-N) γ. Owing to the colossal nitrogen supersaturation, alloy 330 generally possesses significantly higher surface hardness compared to Invar under

equivalent treatment conditions, although the nitrided layers on alloy 330 tend to be thinner than those on Invar after an equivalent TPN treatment.

4 Discussion

4.1 Interstitial nitrogen absorption and lattice expansion

In this study, γ_N denotes the entire group of nitrogen-expanded austenites, with specific phase notation based on the substrate material, such as γ_N-Invar, γ_N-330 and γ_N-316 (formed on Invar 36, alloy RA 330 and AISI 316 ASS, respectively). Comparisons between the γ_N-Invar in this study and the γ_N-330 in Ref. [18] reveal that a significant amount of Cr in the substrate does appear to be conducive to obtaining extremely high levels of interstitial nitrogen incorporation, but is at the same time not a necessity for the nitrogen-induced lattice expansion phenomenon to occur. The γ_N-Invar observed could be classified as $\gamma_{N(i)}$ (i.e. where (i) signifies an absence of strong-nitride-formers in the substrate alloy composition), while the widely-reported interstitial nitrogen-supersaturated and (typically strongly anisotropic) expanded austenite synthesized on Cr-containing ASSs could be denoted as $\gamma_{N(ii)}$. Noticeably, the commercial Invar 36® alloy employed in this study still contains ~0.7 wt.% Cr (and ≤ 0.032 wt.% of Al + Mg + Ti + Zr, see **Table 1**), while the Invar steel substrate used in Ref. [29] (where γ_N-Invar was also synthesized) was reported to contain minor Si content (i.e. ~ 1 at.% of Mn + Si + C).

The terminology of "expanded austenite" was originally introduced to describe austenites with expanded lattice parameters (after nitriding treatments), over those for nitrogen-containing austenite at maximum equilibrium solubility [38]. After the re-definition of "heavily strained austenite" for this terminology [3], expanded austenite are typically used to denote the interstitially-supersaturated (and anisotropically expanded) austenites generally

investigated and reported in the field of Surface Engineering [39]. Nevertheless, expanded austenite, taking the literal meaning of the terminology, includes both $\gamma_{N(i)}$ and $\gamma_{N(ii)}$. With there being no (or much lower amounts of) "nitrogen-trappers" in γ_N-Invar, the route by which $\gamma_{N(i)}$ forms appears to be different to the "nitrogen-trapping" in $\gamma_{N(ii)}$. The ability to accommodate interstitial nitrogen in the parent FCC matrix (with a lattice expansion) typically at non-equilibrium conditions (i.e. low treatment temperatures) arguably depends on the 'chemical environment' (or, as suggested by Dong [22], the electronic structure) provided by the parent alloy with respect to the interstitial species (e.g. N or C atoms), rather than simply the presence of a significant amount of Cr (or another strong-nitride-former).

Interstitial supersaturation is a known (and probably the most essential) feature for $\gamma_{N(ii)}$. As for γ_N-Invar, there is a lack of information on the equilibrium N solubility in γ-Invar and it is still a question, as to whether the γ_N-Invar obtained is N-supersaturated or dissolves nitrogen below the equilibrium solubility limit. Nitrogen solubility in Fe-Ni alloys is known to decease as Ni content increases [40]. According to the partial isothermal section of Fe-Ni-N at 700°C [36], the equilibrium nitrogen solubility drop from ~10 at.% in γ-Fe to ~1 at.% in γ-(Fe, 35Ni). Thus, it is anticipated that the equilibrium nitrogen solubility in γ-Invar will be much lower than that in 'pure' γ-Fe (i.e. ~10.3 at.% N at ~650°C [37]). Nevertheless, the lattice parameters for γ_N-Invar (~0.364 nm at 450°C and up to ~0.368 nm at 400°C, measured from the 111 γ_N-Invar peak positions at ~3 μm depth in **Fig. 4**) are very close to that of γ-Fe with nitrogen at maximum equilibrium solubility (estimated as ~0.365 nm, using $0.3572 + [0.00078 \times at.\%N]$ from Ref. [41]). Given such substantial lattice expansion, the γ_N-Invar obtained is likely N-supersaturated (and could be metastable). However, further study is still required to establish precisely the chemical composition (especially the upper limit of

nitrogen solvation) of γ_N-Invar and to understand the thermodynamic properties of Fe-Ni-N, typically with Ni content close to ~35 at.% Ni and at temperatures below 450°C.

Owing to the different interstitial absorption, one other significant difference between $\gamma_{N(i)}$ and $\gamma_{N(ii)}$ are their lattice expansions observable under XRD. The XRD peak shifts (to lower 2θ angles, with respect to substrate peak positions) of γ_N-Invar are much smaller than those of γ_N-330 after equivalent thermochemical treatments. More importantly, anomalous (anisotropic) lattice expansion, where the XRD peak shift appears significantly larger for 200 reflections than with other hkl planes, is a known signature for the $\gamma_{N(ii)}$ synthesized on ASSs under low-temperature nitriding [7, 11, 17] (as observed also for γ_N-330 [18]). In comparison to $\gamma_{N(ii)}$, γ_N-Invar exhibits an seemingly 'isotropic' lattice expansion − where the observed 111 and 200 XRD peak shifts appear similar after nitrogen-insertion (**Fig. 3**) − for non-stainless austenitic steels under low-temperature nitrogen diffusion treatment. However, taking the GAXRD peak positions (from **Fig. 4**) of substrate γ-Invar and the γ_N-Invar at a depth of ~5 μm, the lattice expansions measured for the 111 and 200 XRD reflections are i) ~1.6% and ~1.8%, respectively, at 400°C and 20hrs, and ii) ~1.1% and ~1.2%, respectively, at 450°C and 20hrs. γ_N-Invar also deviates from an ideal FCC structure, but such deviation appears much less pronounced for γ_N-Invar, presumably owing to the much lower nitrogen absorption levels. Such "slightly distorted FCC structure" of γ_N-Invar could be attributed mainly to the effect of elastic anisotropy of the FCC lattice (with a small compressive stress state) under N-induced lattice expansion. The γ_N-Invar layer synthesized under ion implantation for 15 mins by Williamson et al. [29] is much thinner than the γ_N-Invar layers synthesized under TPN in this study, where the θ-2θ XRD profile of the former covers the entire γ_N-Invar layer and the abovementioned expansion anisotropy was not clearly observed. Furthermore, an "expanded FCC" phase was reported on alloy 330 after hot ammonia

corrosion at 500°C for 1540hrs [42], which was presumed as a nitrogen-containing iron-nickel phase (after the formation of Cr nitride) that may be a phase similar to γ_N-Invar. However, given the white mono-layer shown in cross-section after etching and the absence of CrN under XRD examination of the "corroded" alloy 330 [42], the "expanded FCC" phase on alloy 330 is suspected to be γ_N-330, and probably therefore the first explicit example of $\gamma_{N(ii)}$ published in the open journal literature.

Last but not the least, the 'less expanded FCC structure' on Invar (Fe-35Ni, in [29]) can now be identified as $\gamma_{N(i)}$, being a Cr-free N-expanded austenite. However, Ni-20Fe [29], Fe-30Ni, Fe-32Ni, Fe-42Ni and some FCC Fe-Mn-C steels [19, 20] − as also having Cr-free FCC substrate structure (based on Fe-Ni or Fe-Mn-C system) − showed only a thin γ′ layer without $\gamma_{N(i)}$ under low-temperature nitriding treatments (or nitrogen ion implantation). Nevertheless, detailed structural/compositional information was not provided for the nitrided non-stainless austenitic steels in Ref. [19, 20, 29]. There might be thick γ′ surface layers, such that underlying nitrogen-containing metallic phase(s) were not revealed by XRD. It may be worthwhile to re-visit these alloys (typically the Fe-Ni binary steels with Ni content close to ~35Ni wt.%) under low-temperature thermochemical diffusion treatments. If $\gamma_{N(i)}$ forms only on certain substrate compositions, further study may be required on the electronic structure, bonding states and/or the magnetic properties of γ_N-Invar to elucidate the mechanisms of its formation.

4.2 Decomposition of γ_N

Given the cubic-to-cubic crystallographic orientation relationship between γ′ and γ_N-Invar seen after nitriding at 400°C (**Fig. 5a-c**), the formation of Fe_4N-type γ′ in γ_N-Invar could be realized via diffusion and ordering of the interstitial nitrogen, without the need for

substitutional diffusion. At elevated treatment temperatures, eutectoid decomposition occurs in γ_N-Invar under segregation of substitutional elements (**Fig. 6**). The cellular decomposition morphology of γ_N-Invar appears similar to that of decomposed γ_N-316 [43]. Nevertheless, decomposition products of γ_N-Invar in the cellular regions are Fe_4N-type $\gamma' + \gamma$, whereas for γ_N-316 they are CrN + γ.

One signature feature of $\gamma_{N(ii)}$ is its metastability under paraequilibrium conditions, where the low diffusivity of substitutional elements (e.g. Fe, Cr and Ni) hinders the lattice decomposition mechanisms associated with CrN formation. After TPN at 400°C, no evidence of CrN was found in γ_N-330 [18], whereas γ' forms in γ_N-Invar via interstitial ordering. At slightly higher treatment temperatures (i.e. 425°C and 450°C), the substitutional-diffusion facilitated decomposition occurs more readily in Cr-free γ_N-Invar, compared to γ_N-330. Although $\gamma_{N(i)}$ (e.g. γ_N-Invar) may exhibit significantly lower nitrogen solvency and lattice expansion than $\gamma_{N(ii)}$ (e.g. γ_N-330), the former appears thermodynamically less stable. In this case, Cr atoms in $\gamma_{N(ii)}$ assist in stabilizing the N-rich and expanded FCC structure, by i) providing Cr-N type bonding that competes with the Fe-N type bonding, and ii) providing an extremely slow lattice decomposition mechanism at the low treatment temperatures employed. Future investigations could be performed to address the as yet unanswered questions, as to i) how much “nitrogen-trapper” is required in the substrate alloy composition for the onset of $\gamma_{N(ii)}$ formation after thermochemical diffusion treatment, and ii) whether other strong nitride forming elements could replicate the role of (or replace) Cr in obtaining $\gamma_{N(ii)}$ on austenitic steel substrates. Furthermore, addition of strong nitride forming elements other than Cr could inhibit the formation of CrN in $\gamma_{N(ii)}$ and push the thermal stability of $\gamma_{N(ii)}$ to a higher treatment temperature [44], in which case austenitic metallic substrates alloyed with combinations of strong-nitride forming elements (e.g. Cr, Al, Ti and/or Nb; each

element to no more than a few weight percent) may possess superior thermodynamic stability upon nitrogen supersaturation, enabling higher treatment/service temperature of nitrogen-expanded austenite.

4.3 Nitrogen interstitial diffusion

Comparing the surface nitrogen contents and the hardness-depth profiles between Invar 36 (**Fig. 2a**) and alloy RA 330 (**Fig. 2b**) after TPN treatment, nitrogen atoms were retained at the surface and distributed more homogenously in the relatively thin diffusion layers of $\gamma_{N(ii)}$. However, the high level of Cr content in stainless steel substrates, whilst promoting lattice interstitial supersaturation (and thus superior hardening response), appears also to impede significantly nitrogen inward diffusion, possibly owing to the trapping and detrapping diffusion kinetics proposed in [26]. Noticeably, the Invar 36 substrate contains minor additions of strong nitride formers (e.g. Cr, Al, Ti and Zr, in total below ~0.1 wt.%), which could influence the nitrogen diffusion rate in Invar 36. There should be a threshold concentration level of the strong nitride former (or combinations thereof) in austenitic steel, above which interstitial diffusion in the austenite matrix slows down and nitrogen atoms are retained at the surface owing to the 'trap effect'.

Comparing thermochemical diffusion treatments of AISI 316 ASS by nitrogen (γ_N-316) or carbon (γ_C-316) in literature (the alloy for which probably the most extensive prior published data exists), γ_N-316 layers possess composition-depth profiles with a high nitrogen plateau followed an abrupt drop in nitrogen content at the diffusion layer front (with corresponding lattice expansions and hardness/depth profiles) [35, 45, 46], while the carbon concentration (and corresponding lattice expansion and hardness) in γ_C-316 layers is normally lower and with a smoothly-reducing depth profile towards the substrate core [8, 45-47]. As for the

chemically-homogenous γ_C-316 and γ_N-316 powders, carbon absorption of γ_C-316 ranges from 0 to ~18 at.% [48, 49], while γ_N-316 has been shown to possess a lower limit of interstitial nitrogen solvation (e.g. ~14-38 at.% N [10]). For the γ_N-Invar zones observed in this study, the continuous lattice expansion from the unmodified core (**Fig. 4**) and the smoothly reducing hardness-depth profiles (**Fig. 2a**) hints at there being no lower interstitial solvation limit – and the smoothly reducing nitrogen depth profile appears very different to γ_N-316 (but somewhat similar to γ_C-316). The abovementioned differences between γ_N-316 (as a type of $\gamma_{N(ii)}$) and γ_N-Invar (as a type of $\gamma_{N(i)}$), which could be associated to the strong chemical affinity between Cr and N, confirm the influence from the 'chemical environment' of the substrate alloy (e.g. with or without Cr) on the absorption of interstitial N during thermochemical diffusion treatments.

4.4 Nitrogen interstitial ordering

Compared to FCC-γ, one distinctive feature of γ′ is the nitrogen interstitial ordering, where the 'inserted' N atoms occupy the body centres, i.e. $\frac{1}{2}\ \frac{1}{2}\ \frac{1}{2}$, of the host FCC cubes. Such interstitial ordering give rise to the extra 'forbidden' FCC reflections in EDPs (compare **Fig. 5b1-2** and **Fig. 5c1-2**) and the γ′(110) peak under XRD (**Fig. 3b)**. These extra diffraction reflections are also widely observed for $\gamma_{N(ii)}$ layers, reported under both electron diffraction (e.g. in γ_N-316 [50, 51], γ_N-304 [52] and γ_N-AG17 [18]) and XRD (i.e. γ_N-316 [53]). These reflections are not observed in $\gamma_{N(ii)}$ when nitrogen content is low [18, 51] and are only observed under XRD when the nitrogen content is extremely high (i.e. for the 'chemically-homogenous' γ_N-316 powders containing ~35.5 at.% N [53]). With increasing nitrogen content, $\gamma_{N(ii)}$ could show i) no forbidden FCC reflections (at low N content), ii) forbidden reflections under electron diffraction (potentially owing to nitrogen-interstitial ordered domains [51] at intermediate-to-high N content), and iii) forbidden reflections under X-ray

diffraction (owing to long-range ordering of interstitial nitrogen [53] under extreme conditions of high N uptake). More importantly, Cr-containing Fe_4N-like γ′ phases [54] were reported in the $\gamma_{N(ii)}$ formed on Fe-Cr-Ni alloys, typically at the topmost surface (with the highest nitrogen concentration). The Cr-containing Fe_4N-like γ′ in $\gamma_{N(ii)}$ is somewhat comparable to the uniform Cr-free Fe_4N-type γ′ in $\gamma_{N(i)}$, that both of them could form via interstitial diffusion and/or ordering of nitrogen at low treatment temperature. In this regard, $\gamma_{N(ii)}$ could exhibit either a random solid solution of N, short-range-ordering of N or long-range-ordering of N, depending on the local nitrogen concentration. The exact position of N in $\gamma_{N(ii)}$ is so far unclear and should vary at different stages of nitrogen absorption level, but it is most likely that N atoms are 'trapped' at octahedral interstices near substitutional Cr atoms in the FCC unit cell. In contrast, the $\gamma_{N(i)}$ in this study does not present extra 'forbidden' diffraction signals either under electron diffraction nor by XRD, i.e. there is no evidence of any interstitial ordering. A Fe-Ni-N solid solution is anticipated for $\gamma_{N(i)}$, with nitrogen atoms occupying randomly some fraction of the octahedral interstices.

Conclusions

Further to a previous study on the role of Mn and Ni in the formation and structure of nitrogen-expanded austenite on ASSs, another (and arguably more important) aspect, on the role of Cr in the formation of γ_N (and/or on the alloy selection/design criteria for nitrogen interstitially-expandable steels/alloys), is discussed in present work. Comparing to the anisotropic nitrogen-expanded austenite $\gamma_{N(ii)}$ (e.g. γ_N-330 that formed on 330 alloy), an almost isotropic nitrogen-expanded austenite $\gamma_{N(i)}$ (viz. γ_N-Invar) is revealed on a non-stainless austenitic steel (Invar 36®) after TPN treatment, showing very different lattice expansion and surface hardening behavior. Cr-alloying in austenitic steel substrates is an important factor in obtaining colossal nitrogen interstitial supersaturation; but the occurrence

of interstitial-induced lattice expansion under low temperature nitrogen thermochemical diffusion treatment does not required a significant content of Cr in substrate.

The γ_N-Invar diffusion zones, although providing less of a hardening effect, are much thicker than those on γ_N-330. Comparing the decomposition between γ_N-330 and γ_N-Invar, the presence of Cr-alloying appears beneficial in suppressing the formation of γ'-Fe_4N type iron nitrides and enhancing the thermodynamic stability of γ_N. This implies a need for further study on the contents of nitride-forming elements required in austenitic alloys (or austenite-containing duplex or precipitation-hardening alloy) to effectively 'trap' interstitial N atoms for optimum nitrogen absorption during low-temperature diffusion treatment (i.e. to maximize – and stabilize – γ_N formation, whilst retaining high nitrogen interstitial inward diffusion rates for hard and thick treatment layers). For example, austenitic metallic matrices (e.g. Ni or Fe-Ni/Mn) alloyed with (combinations of) strong nitride-forming elements could be evaluated under different low-temperature nitriding conditions, to explore the optimal balance between treatment efficiency and treatment layer stability.

Acknowledgement

This research did not receive any specific grant from funding agencies in the public, commercial, or not-for-profit sectors. We would however like to thank City Special Metals Ltd. (Sheffield, UK) for the provision of alloy Invar® 36 for this study.

References

[1] Z.L. Zhang, T. Bell: Surf. Eng., 1985, vol. 1, pp. 131-136.

[2] K. Ichii, K. Fujimura, T. Takase: Technol. Rep. Kansai Univ., 1986, vol. 27, pp. 135-144.

[3] A. Leyland, D.B. Lewis, P.R. Stevenson, A. Matthews: Surf. Coat. Technol., 1993, vol. 62, pp. 608-617.

[4] D.B. Lewis, A. Leyland, P.R. Stevenson, J. Cawley, A. Matthews: Surf. Coat. Technol., 1993, vol. 60, pp. 416-423.

[5] A. Matthews, A. Leyland: Mater. Sci. Forum, 1994, vol. 163-165, pp. 497-508.

[6] Y. Sun, T. Bell: Wear, 1998, vol. 218, pp. 31-42.

[7] Y. Sun, X.Y. Li, T. Bell: J. Mater. Sci., 1999, vol. 34, pp. 4793-4802.

[8] Y. Cao, F. Ernst, G.M. Michal: Acta Mater., 2003, vol. 51, pp. 4171-4181.

[9] S. Collins, P. Williams, Advanced Materials and Process, ASM International, 2006, pp. 32-33.

[10] T. Christiansen, M.A.J. Somers: Metall. Mater. Trans. A, 2006, vol. 37A, pp. 675-682.

[11] T. Christiansen, M.A.J. Somers: Scripta Mater., 2004, vol. 50, pp. 35-37.

[12] T. Christiansen, M.A.J. Somers: Z. Metallkd., 2006, vol. 97, pp. 79-88.

[13] J. Buhagiar, X. Li, H. Dong: Surf. Coat. Technol., 2009, vol. 204, pp. 330-335.

[14] J.C. Stinville, P. Villechaise, C. Templier, J.P. Riviere, M. Drouet: Acta Mater., 2010, vol. 58, pp. 2814-2821.

[15] C. Templier, J.C. Stinville, P. Villechaise, P.O. Renault, G. Abrasonis, J.P. Riviere, A. Martinavicius, M. Drouet: Surf. Coat. Technol., 2010, vol. 204, pp. 2551-2558.

[16] F.A.P. Fernandes, T.L. Christiansen, G. Winther, M.A.J. Somers: Acta Mater., 2015, vol. 94, pp. 271-280.

[17] B.K. Brink, K. Stahl, T.L. Christiansen, J. Oddershede, G. Winthiner, M.A.J. Somers: Scripta Mater., 2017, vol. 131 pp. 59-62.

[18] X. Tao, X. Liu, A. Matthews, A. Leyland: Acta Mater., 2019, vol. 164, pp. 60-75.

[19] E. Menthe, K.T. Rie, J.W. Schultze, S. Simsson: Surf. Coat. Technol., 1995, vol. 74-75, pp. 412-416.

[20] N. Yasumaru: Mater. Trans., JIM, 1998, vol. 39, pp. 1046-1052.

[21] D.L. Williamson, I. Ivanov, R. Wei, P.J. Wilbur: Mater. Res. Soc. Symp. Proc., 1992, vol. 235.

[22] H. Dong: Int. Mater. Rev., 2010, vol. 55, pp. 65-98.

[23] R.B. Frandsen, T. Christiansen, M.A.J. Somers: Surf. Coat. Technol., 2006, vol. 200, pp. 5160-5169.

[24] J. Lutz, J.W. Gerlach, S. Mandl: Phys. Status Solidi A, 2008, vol. 205, pp. 980-984.

[25] D.L. Williamson, J.A. Davis, P.J. Wilbur, J.J. Vajo, R. Wei, J.N. Matossian: Nucl. Instrum. Methods Phys. Res., Sect. B, 1997, vol. 127-128, pp. 930-934.

[26] S. Parascandola, W. Moller, D.L. Williamson: Appl. Phys. Lett., 2000, vol. 76, pp. 2194-2196.

[27] J.P. Riviere, M. Cahoreau, P. Meheust: J. Appl. Phys., 2002, vol. 91, pp. 6361-6366.

[28] J. Oddershede, T.L. Christiansen, K. Stahl, M.A.J. Somers: Scripta Mater., 2010, vol. 62, pp. 290-293.

[29] D.L. Williamson, J.A. Davis, P.J. Wilbur: Surf. Coat. Technol., 1998, vol. 103-104, pp. 178-184.

[30] F. Pedraza, C. Savall, G. Abrasonis, J.P. Riviere, J.F. Dinhut, J.L. Grosseau-Poussard: Thin Solid Films, 2007, vol. 515, pp. 3661-3669.
[31] T. Makishi, K. Nakata: Metall. Mater. Trans. A, 2004, vol. 35A, pp. 227-238.
[32] M. Fonovic, A. Leineweber, O. Robach, A. Jagle, E.J. Mittemeijer: Metall. Mater. Trans. A, 2015, vol. 46A, pp. 4115.
[33] A. Leyland, K.S. Fancey, A.S. James, A. Matthews: Surf. Coat. Technol., 1990, vol. 41, pp. 295-304.
[34] A. Leyland, K.S. Fancey, A. Matthews: Surf. Coat. Technol., 1991, vol. 7, pp. 207-215.
[35] M.A.J. Somers, T. Christiansen: Gaseous processes for low temperature surface hardening of stainless steel, in: E.J. Mittemeijer, M.A.J. Somers (Eds.) Thermochemical Surface Engineering of Steels, 1st ed., Woodhead Publishing, Cambridge, 2015, pp. 581-614.
[36] P. Perrot: Iron - Nitrogen - Nickel, in: G. Effenberg, S. Ilyenko (Eds.) Landolt-Bornstein - Group IV Physical Chemistry (Numerical Data and Functional Relationships in Science and Technology), Vol. 11D, Part 4, 1st ed., Springer, Berlin, Heidelberg, 2008.
[37] H.A. Wriedt, N.A. Gokcen, R.H. Nafziger: Bull. Alloy Phase Diagrams, 1987, vol. 8, pp. 355.
[38] S.P. Hannula, O. Nenonen: Thin Solid Films, 1989, vol. 181, pp. 343-350.
[39] M.A.J. Somers, T. Christiansen: Low temperature surface hardening of stainless steel in: E.J. Mittemeijer, M.A.J. Somers (Eds.) Thermochemical Surface Engineering of Steels, 1st ed., Woodhead Publishing, Cambridge, 2015, pp. 557-579.
[40] D. Atkinson, C. Bodsworth: J. Iron Steel Inst., London, 1970, vol. 208, pp. 587-593.
[41] D. H. Jack, K.H. Jack: Mater. Sci. Eng., 1973, vol. 11, pp. 1-27.
[42] J.J. Moran, J.R. Mihalisin, E.N. Skinner: Corrosion, 1961, vol. 17, pp. 191t-195t.
[43] X.Y. Li, Y. Sun: Transmission electron microscopy study of S phase in low temperature plasma nitrided 316 stainless steel, in: T. Bell, K. Akamatsu (Eds.) Stainless Steel 2000: Thermochemical Surface Engineering of Stainless Steel, 1st ed., Maney Publishing, London, 2001, pp. 215-228.
[44] T. Christiansen, K.L. Dahm, M.A.J. Somers: BHM Berg- und Hüttenmännische Monatshefte, 2015, vol. 160, pp. 406-412.
[45] T. Christiansen, M.A.J. Somers: Surf. Eng., 2005, vol. 21, pp. 445-455.
[46] S. Thaiwatthana, X.Y. Li, H. Dong, T. Bell: Surf. Eng., 2002, vol. 18, pp. 433-437.
[47] G.M. Michal, F. Ernst, H. Kahn, Y. Cao, F. Oba, N. Agarwal, A.H. Heuer: Acta Mater., 2006, vol. 54, pp. 1597-1606.
[48] T.L. Christiansen, K. Stahl, B.K. Brink, M.A.J. Somers: Steel Res. Int., 2016, vol. 87, pp. 1395-1405.
[49] T.S. Hummelshoj, T.L. Christiansen, M.A.J. Somers: Scripta Mater., 2010, vol. 63, pp. 761-763.
[50] D. Stroz, M. Psoda: J. Microsc. (Oxford, U. K.), 2010, vol. 237, pp. 227-231.
[51] J.C. Jiang, E.I. Meletis: J. Appl. Phys., 2000, vol. 88, pp. 4026-4031.
[52] K. Tong, F. Ye, H. Che, M.K. Lei, S. Miao, C. Zhang: J. Appl. Crystallogr., 2016, vol. 49, pp. 1967-1971.
[53] B.K. Brink, K. Stahl, T. Christiansen, C. Frandsen, M.F. Hansen, M.A.J. Somers: Acta Mater., 2016, vol. 106, pp. 32-39.
[54] H.L. Che, S. Tong, K.S. Wang, M.K. Lei, M.A.J. Somers: Acta Mater., 2019, vol. 177, pp. 35-45.

Appendix

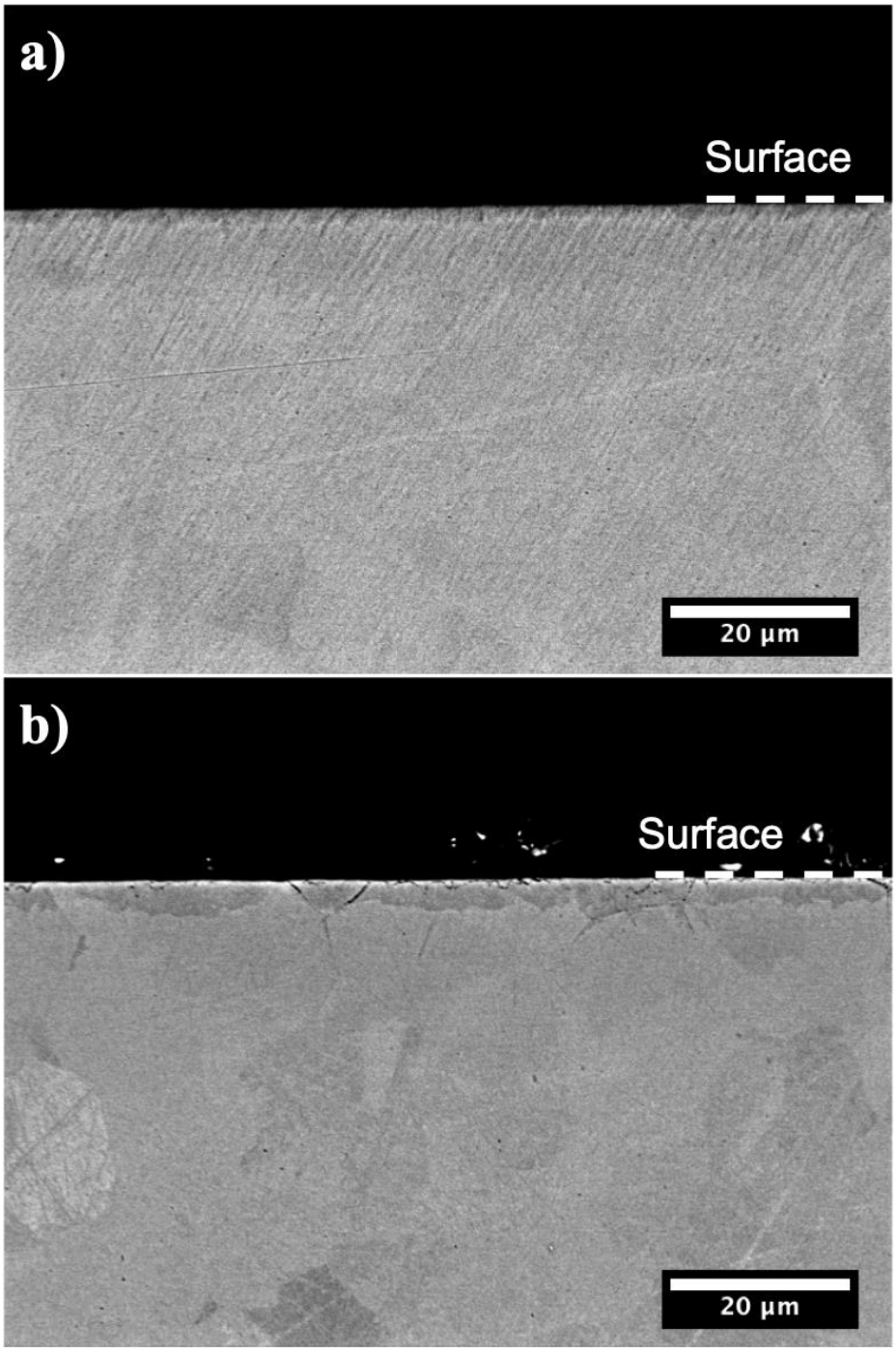

Figure A1 Cross-sectional BSE images of Invar 36® after plasma nitriding at a) 400°C and b) 450°C for 20hrs, at a low magnification to cover the entire hardened zones. No clear features were found corresponding to γ_N-Invar. The "grain structure"

641 observed is most likely owing to different BS electron scattering behavior to different
642 grain orientation.